Assessment of thermal effects in a model of the human head implanted with a wireless active microvalve for the treatment of glaucoma creating a filtering bleb

F Schaumburg and F A Guarnieri

CIMEC Centro de Investigacin de Mtodos Computacionales, UNL, CONICET, Col. Ruta 168 s/n, Predio Conicet Dr Alberto Cassano, 3000 Santa Fe, Argentina
Facultad de Ingeniera, UNER, Ruta Provincial 11 Km 10, 3100 Oro Verde, Argentina

E-mail: fschaumburg@bioingenieria.edu.ar

December 2016

Abstract. A 3D anatomical computational model is developed to assess thermal effects due to exposure to the electromagnetic field required to power a new investigational active implantable microvalve for the treatment of glaucoma. Such device, located in the temporal superior eye quadrant, produces a filtering bleb which is included in the geometry of the model, together with relevant ocular structures. The electromagnetic field source, a planar coil, and the microvalve antenna and casing are also included. Exposure to the electromagnetic field source of an implanted and a non-implanted subject are simulated by solving a magnetic potential formulation, using the finite element method. Maximum SAR_{10} is reached in the eyebrow and remains within the limits suggested by IEEE and ICNIRP standards. The anterior chamber, filtering bleb, iris and ciliary body are the ocular structures more absorption occurs. Temperature rise distribution is also obtained by solving the bioheat equation with the finite element method. Numerical results are compared with in vivo measurements obtained from four rabbits implanted with the microvalve and exposed to the electromagnetic field source.

1. Introduction

Glaucoma is a group of ocular diseases affecting approximately 70 million people worldwide, leading to irreversible blindness due to the damage caused to the optic nerve by the increased intraocular pressure. Glaucoma is first treated pharmacologically with agents that either lower aqueous humor production or increase aqueous humor drainage. When these treatments are not effective, surgical procedures such as trabeculoplasty and trabeculectomy are indicated. Another option are aqueous shunts, which are passive implantable devices used to drain aqueous humor underneath the conjunctiva, where it is absorbed. Several issues have been reported regarding aqueous shunts, i.e. postoperative

hypotony and fibrosis (Lim et al. 1998, Schwartz et al. 2006, Goel et al. 2010, Weinreb et al. 2014).

As an alternative, an active implantable microvalve for glaucoma called iMvalv is described in Guarnieri (2012). As well as aqueous shunts, this microvalve is placed in the temporal superior eye quadrant, in a pocket created surgically in conjunctival tissue, which gets filled by aqueous humor, creating a so called *filtering bleb*. The principle of this active valve is to regulate the intraocular pressure by means of an electroactive polymer which deforms to an electric signal, allowing to control the amount of aqueous humor drained into the bleb. Such actuator allows to respond to hypotony, as well as to satisfy the patients particular draining requirements. The implantable device (or internal unit) has a planar coil antenna, which couples to another planar coil antenna included in an external unit for powering. This inductive coupling is tuned to 13.56 MHz. More information about the iMvalv operation and filtering blebs can be found in Sassetti et al. (2012), Torres & Guarnieri (2015) and Greenfield et al. (1998).

In order to guarantee that this device is safe to be operated, it is necessary to assess the side effects due to exposure to the external unit electromagnetic field (EMF). The Institute of Electrical and Electronics Engineers (IEEE) and the International Commission on Non-Ionizing Radiation Protection (ICNIRP), established limits for electromagnetic exposure taking into consideration known adverse health effects. At the working frequency (13.56 MHz) restrictions are placed on the Specific Absorption Rate (SAR) and are intended to prevent whole body heating stress and excessive localized tissue heating. Specifically, for 10 MHz to 10 GHz exposure these standards recommend that SAR, averaged over 10 grams of tissue (SAR_{10}), should remain below 2 W/Kg for general public. However, medical applications are out of the scope of these standards. Regarding eye exposure to RF, adverse effects ranging from cell disruption to vision loss were reported. Nonetheless, the only established adverse effect due to localized exposure is cataract formation in rabbits, due to heating, associated to temperatures $\geq$41 °C in the lens (Elder 2003, Vander Vorst et al. 2006). Power applied into retinal tissue should also be accounted for, since retinal damage was reported when a 50 mW heat source was directly applied over a 1.4 mm^2 area for more than one second (Margalit et al. 2002). Thus, although medical applications are not reached by the named standards, they should be accounted for anyway, because the device under study requires exposure on daily basis, and it is desirable to limit tissue heating. Moreover, ICNIRP (1998) and IEEE (2005) limits are strict, and do not allow temperature rises as big as 41 °C, reported to cause cataracts. Besides, the power density reported to cause retinal damage ($\approx$36000 W/m^2) is far from ICNIRP reference levels for 13.56 MHz exposure (2 W/m^2).

SAR can be calculated with the aid of computational models. Other authors already developed computational models to assess exposure in people wearing active ocular wireless devices. Ng et al. (2011), DeMarco et al. (2003), Gosalia et al. (2004) and Singh et al. (2009) assessed exposure of subjects wearing retinal prostheses powered via inductive links in the 1-10 MHz range. Similarly, Hirtl & Schmid (2013) developed a model for subjects wearing an intraocular pressure sensor powered with an inductive

coupling working at 13.56 MHz. Additionally, although less similar to this work, other studies involving ocular tissue exposure to EMF sources such as mobile devices and wireless networks, are Taflove & Brodwin (1975), Bernardi et al. (1998), Hirata et al. (2000), Hirata (2005), and Buccella et al. (2007). However, EMF distributions are highly dependant on problem geometry, and the position of the microvalve as well as the geometries of the internal and external antennae, differ from other authors' studies. Moreover, retinal implants and intraocular pressure sensors do not involve the creation of a filtering bleb.

The named standards were developed taking into consideration established adverse health effects due to EMF exposure, but didnt take into account physiopathological structures such as filtering blebs. The presence of a filtering bleb in a dosimetric study is of much relevance, because it has a volume comparable to the eye anterior chamber, it is close to the external unit antenna, and it is filled with aqueous humor, which has high electrical conductivity and is expected to absorb RF energy significantly. Besides, the reference level given by ICNIRP for the **H**-field at 13.56 MHz is 0.073 A/m. Currents driving the external unit antenna, are expected to be 1 A or greater, generating magnetic fields bigger than this reference level by several orders of magnitude, near the antenna. Because the implantable unit and the filtering bleb can be as close as 1 cm to the external antenna, then it is not obvious that basic restrictions will not be surpassed. Furthermore, the necessity of improving the performance of the drainage devices has been detected by many research groups, trying passive (Diouf et al. 2008) and active approaches (Neagu 1998, Bae et al. 2003, Pan et al. 2007, Stergiopulos 2016). As long as new drainage devices are located in the same place than traditional aqueous shunts, the subconjunctival space, they will create a filtering bleb. Additionally, if this new devices are powered inductively or if they transmit information telemetrically, they will involve the exposure of the filtering bleb to electromagnetic radiation. In this context, a dosimetric study involving a filtering bleb must be undertaken, to determine whether the named microvalve is safe to be operated, and to set a precedent for future ocular devices.

This work presents a computational 3D anatomical model including the implantable device and filtering bleb, developed to assess thermal effects due to the EMF required to power the mentioned novel implantable microvalve. To calculate SAR, a formulation for the magnetic potential derived from Maxwells equations, is solved numerically using the Finite Element Method (FEM). That formulation is benchmarked using a problem with a known analytical solution. The anatomical model is used to simulate exposure to the external unit EMF of both implanted and non-implanted subjects. Results of those scenarios are compared to evaluate the internal unit and bleb effect. Furthermore, temperature increase (ΔT) is calculated in order to compare with *in* vivo measurements, obtained from four rabbits implanted with the microvalve. The Pennes bioheat equation is solved for temperature calculation. SAR maximum values are compared with ICNIRP and IEEE recommendations. Finally, basal temperature distribution is compared with other authors experimental results, and a mesh convergence study is undertaken.

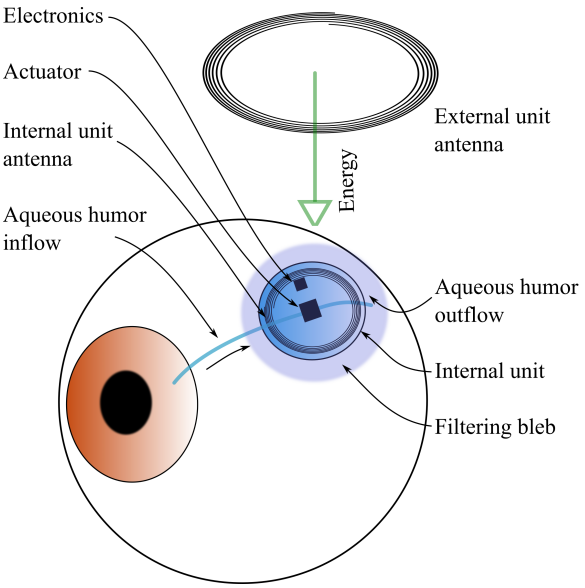

Figure 1: A block diagram of the iMvalv system.

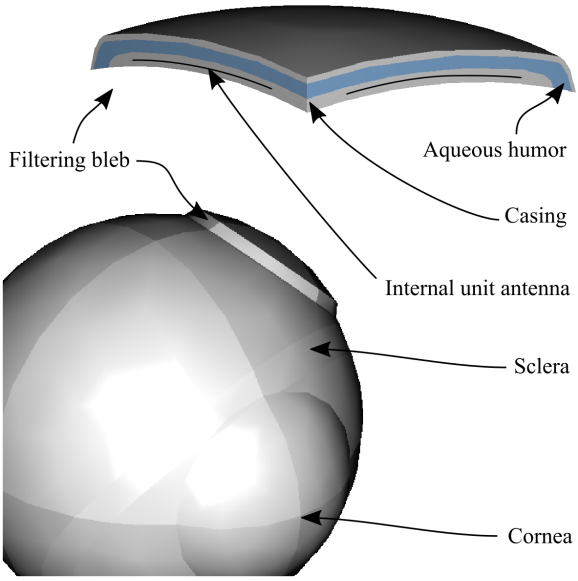

Figure 2: Geometries of the eye, the filtering bleb and the internal unit, used for the electromagnetic and thermal models.

2. Methods and models

2.1. System description

As mentioned, the complete system consists of an external unit and an internal implantable unit linked through an inductive coupling tuned to 13.56 MHz. Antennae are separated from one another by 1.2 cm and work with a 100% duty cycle. The external unit provides the energy the internal unit requires for operation. Duration of exposure is proportional to the amount of aqueous humor to be drained into the bleb. The internal unit is made of a flexible substrate where the actuator and the electronics lie, all surrounded by a polydimethylsiloxane (PDMS) casing. The electroactive polymer actuator is driven by a control signal generated by an electronic circuit, starting from the electromagnetic energy received by the antenna. Aqueous humor enters the actuator after passing through a cannula inserted in the anterior chamber of the eye, and reaches the filtering bleb after exiting the actuator. A diagram of all the system of the microvalve can be seen in figure 1.

2.2. Anatomical geometry

The model geometry is composed of a human head where the eye socket and eye structures are represented in more detail. The microvalve and its external unit are also included. Eye structures were created starting from a tomographic sketch taken from DeMarco et al. (2003), later revolved in order to obtain a 3D object. A

Table 1: Tissue and material properties.

Tissue	σ [S/m]	ε_r	K [W/(m°C)]	B [J/(s°Cm^3)]	A [W/m^3]
Aqueous humor	1.502	69.697	0.58	0	0
Bone	0.045	30.575	0.40	1000	0
Choroids	1.117	210.64	0.51	85000	20000
Conjunctival	0.812	162.19	0.58	0	0
Cornea	0.812	162.19	0.58	0	0
Filling tissue	0.327	153.12	0.57	35000	10000
Lens	0.534	134.49	0.40	0	0
Ciliary body	0.628	138.44	0.5	2700	690
Orbital fat	0.030	11.827	0.25	520	180
Retina	0.812	162.19	0.56	9500	2500
Sclera	0.812	162.19	0.58	0	0
Vitreous humour	1.502	69.697	0.58	0	0
Air	0	1	0.026	0	0
PDMS	0	2.5	0.15	0	0

Conjunctival tissue was treated as scleral. Head filling tissue was represented by the most abundant head tissue: white and grey matter. Air and PDMS electrical conductivities were rounded to zero.

similar approach was followed for the eye socket bones, orbital fat, and the optic nerve. The filtering bleb was placed in the temporal superior eye quadrant. The head shape was taken from the IEEE specific anthropomorphic mannequin for SAR measurement (IEEE 2003). The internal unit antenna, a nine-turn-octogonal-planar coil, is modeled as a circular-annular surface, respecting its inner diameter (1.6 mm) and outer diameter (8.2 mm). That antenna is surrounded by the 250 µm thick casing. Similarly, the external unit antenna, a rectangular ten-turn-planar coil with inner and outer sides 5 mm and 54 mm, is modeled as a flat rectangular annular surface. The air domain is a 80 cm cube. The geometries of the eye, the filtering bleb and the internal unit, can be seen in figure 2.

2.3. Tissue and material properties

Electromagnetic and thermal properties of tissue and used material are listed in table 1, where σ is the electrical conductivity, ϵ_r is the relative permittivity, K is the thermal conductivity, B is the blood perfusion and, A is the metabolic rate. Tissue thermal properties were taken from Buccella et al. (2007) while electromagnetic properties from an online tool provided by the Italian National Research Council (IFAC 1997). Air properties were chosen from Lide (2004), while PDMS properties from Kuo (1999).

2.4. SAR Calculation

The specific absorption rate is a measure of the rate at which energy is absorbed in body tissue. For harmonically varying EMF is defined as $SAR = \frac{\sigma}{2\rho} |\mathbf{E}|^2$.

In order to obtain the EMF in each point of the geometry, a formulation for the magnetic potential $\mathbf{A}$, was solved:

$$\left(j\omega\sigma - \omega^2\varepsilon\right)\mathbf{A} + \nabla \times \left(\frac{\nabla \times \mathbf{A}}{\mu}\right) = \mathbf{0} \tag{1}$$

where ω is the angular frequency and μ is the magnetic permeability. Equation 1 can be obtained by replacing in the Ampere's Law for harmonic fields the constitutive relations for linear isotropic materials and the definitions of electric and magnetic potentials. The magnetic insulation boundary condition ($\mathbf{n} \times \mathbf{A} = \mathbf{0}$) was used in the exterior boundaries. In the internal antenna surface, a sheet impedance boundary condition ($\eta\mathbf{n} \times (\mathbf{H}_1 - \mathbf{H}_2) = \mathbf{n} \times (\mathbf{n} \times \mathbf{E})$) was used. The used surface impedance η value is discussed in section 2.6. In the external antenna, a surface current density $\mathbf{J}_\mathrm{s}$ was prescribed ($\mathbf{n} \times (\mathbf{H}_1 - \mathbf{H}_2) = \mathbf{J}_s$) in order to produce at least a 1.4 mA current in the internal antenna, which is the minimum current needed for operation. Finally, a continuity boundary condition ($\mathbf{n} \times (\mathbf{H}_1 - \mathbf{H}_2) = \mathbf{0}$) was used in the remaining interior interfaces (Jin 2002). To obtain the SAR distribution in a non-implanted subject, the material of subdomains associated to the microvalve and filtering bleb, were replaced by orbital fat. The described electromagnetic problem was solved numerically using the finite element method with COMSOL Multiphysics finite element environment. Geometry was meshed with 1703136 second order tetrahedral elements. The biconjugate gradient stabilized iterative method (BiCGStab) was used as a solver with the symmetric successive overrelaxation method (SSOR) as preconditioner.

2.5. Analytical and FEM comparison

Results obtained with 1 and FEM were tested with a problem with a known analytical solution, presented in Singh et al. (2009): the **E**-field distribution of a 10 turn-spiral planar coil with external diameter 39 mm and internal diameter 21.5 mm, when excited with a 10 MHz signal. The **E**-field magnitudes obtained analytically and with FEM were compared.

2.6. Annular coil simplification

Multiple-turn coils as shown in figure 3a require a fine mesh with many elements, producing an unnecessarily large FEM problem. To stay within the limits of the available resources, both internal unit and external unit antennae were modeled as annular instead of multiple turns, as shown in figure 3b. Other authors who dealt with the same problem, with a similar approach, are Ng et al. (2011) and Hirtl & Schmid (2013). The error produced by such simplification was studied by solving auxiliary 3D models. To study the error produced by the annular simplification in the external antenna, the **E**-field produced by a unitary superficial current was obtained with the real-multiple-turn geometry and with the annular geometry, and compared. The error produced by the annular simplification in the internal antenna was also assessed. First, the

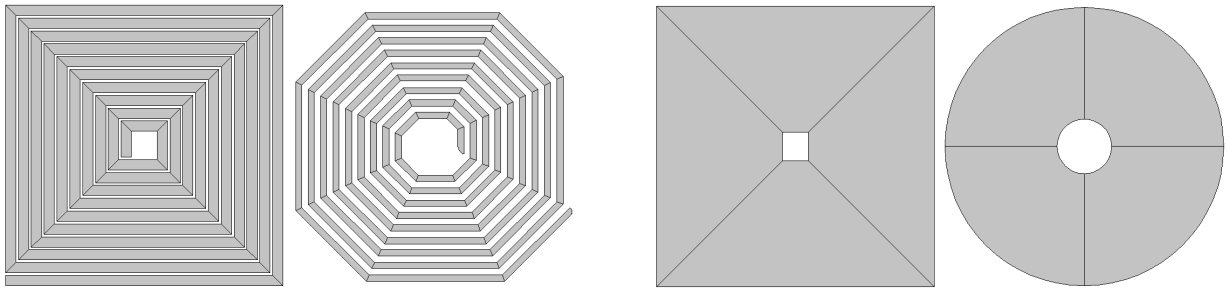

(a) (b)

Figure 3: (a) Real multiple turn coil antennae and (b) annular coil antennae simplification (figures out of scale).

surface impedance in the internal-multiple-turn antenna η_{MT}, was chosen to produce an impedance matching the impedance of the implant electronics. This equals (875+135j) Ω at the working frequency. The induced current $\mathrm{I_{MT}}$ was obtained for exposure to the EMF produced by the external-annular antenna excited with a unitary surface current. The surface impedance in the internal-annular antenna η_{A}, was tuned to produce a current equal to $\mathrm{I_{MT}}$ when exposed to the same EMF. The magnitude of the **E**-field in the proximities of the annular and multiple-turn internal antennae were compared.

2.7. ΔT Calculation

For calculating temperature distribution in both exposed and basal state, the Pennes Bioheat Equation was used:

$$\rho C \frac{\partial T}{\partial t} = \nabla \cdot (K \nabla T) + A + B\,(T - T_{blood}) + \rho SAR \tag{2}$$

where the term in the left represents dynamic temperature rise, the first term on the right is thermal spatial diffusion, the second is the metabolic heat source, the third represents the heat dissipation due to blood perfusion, and the last term represents the heat source due to EMF exposure, and couples the electromagnetic and thermal problems. A convective boundary condition ($\mathbf{n} \cdot (K_1 \nabla T_1 - K_2 \nabla T_2) = H\,(T - T_{room})$) was used in the air interfaces, with convective coefficients H of 10.5 $\mathrm{W/m^{2\circ}C}$ in the skin/air interface, and 20 $\mathrm{W/m^{2\circ}C}$ in the cornea/air interface (Buccella et al. 2007). Heat flux continuity ($\mathbf{n} \cdot (K_1 \nabla T_1 - K_2 \nabla T_2) = 0$) was set in the remaining interior interfaces. Room temperature was fixed to $\mathrm{T_{room}} = 24\ ^{\circ}\mathrm{C}$ on the exterior boundaries. More detailed description of 2 and its boundary conditions can be found in Lazzi (2005). To obtain steady state temperature distribution for the exposed subject, 2 was solved without the dynamic term. Additionally, to obtain basal temperature distribution the EMF heat source term was suppressed. Finally, temperature rise distribution was calculated as temperature in the exposed scenario minus temperature in the basal state. The described thermal problem was solved with FEM using the mesh and solver described in section 2.4.

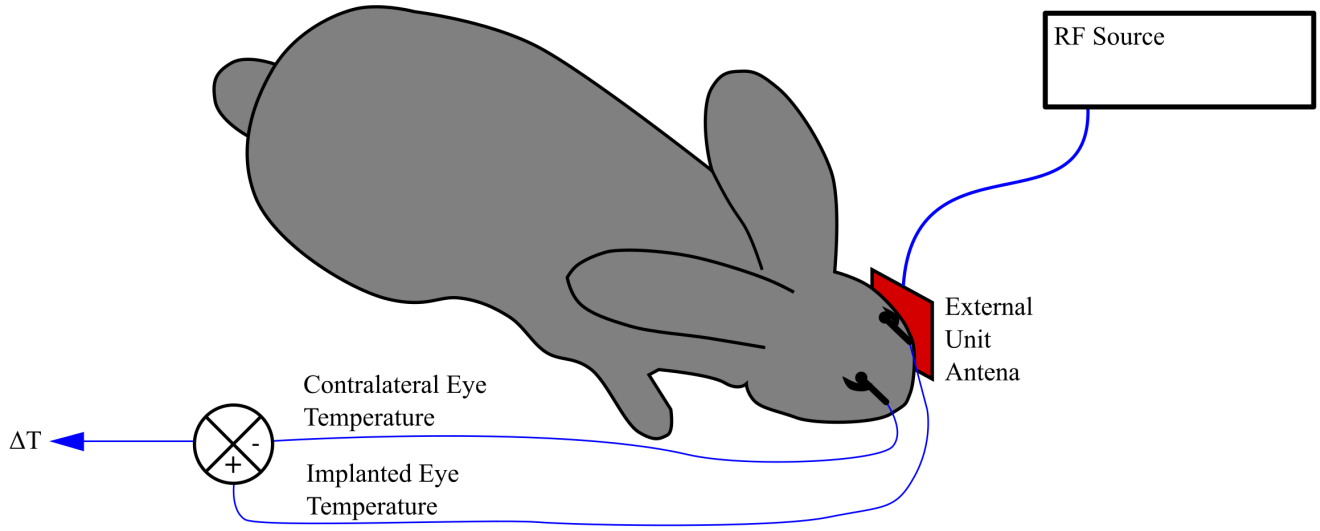

Figure 4: Experimental setup for measuring temperature rise implanted rabbits.

2.8. Basal temperature comparison

Average corneal basal temperature T_{av} and its standard deviation SD were calculated from experimental results obtained by 21 authors whose results were compiled in Ng & Ooi (2007). Those results were compared with corneal basal temperature obtained numerically T_{FEM}.

2.9. Temperature rise measurement in rabbits

Temperature rise was measured in the eyebrow of four sedated New Zealand male rabbits wearing the microvalve in an operating room at the *Centro de Medicina Comparada*, ICiVet Litoral, R.P. Kreder 2805, S3080HOF Esperanza, Santa Fe, Argentina. Rabbits were exposed for a 20 minute period to the external unit EMF. A BK-Precision 4040 signal generator was used to generate a 13.56MHz continuous wave signal, producing a 0.44 ampere-turn magnetomotive force in the external antenna. Because the signal-to-noise ratio was expected to be low, two NTC temperature sensors with 0.05 °C accuracy were used in a differential configuration. Temperature rise was calculated as temperature in the implanted eye minus temperature in the contralateral eye. This configuration compensates changes in room temperature, and in the rabbit core temperature and is shown in figure 4.

2.10. Mesh convergence study

To find out if the obtained results depend on the mesh used, a mesh convergence study was undertaken. Five meshes with degrees of freedom among 115665 and 10818974 were used. The **E**-field magnitudes along an axis, from the center of the cornea to the retina, were compared. Results presented in section 3 correspond to the finest mesh.

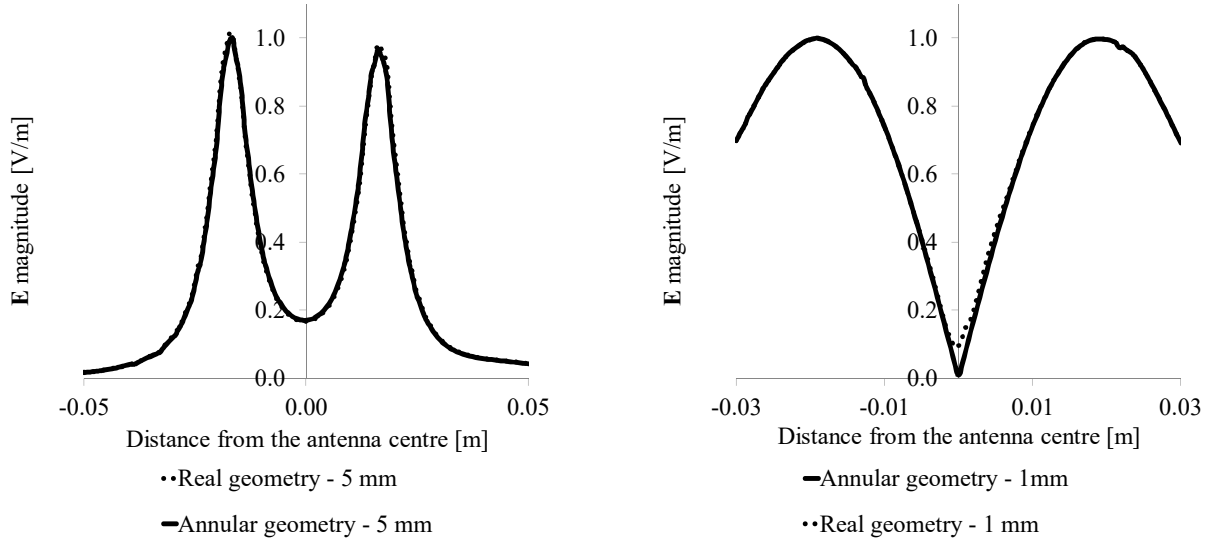

(a) (b)

Figure 5: Normalized **E**-field magnitudes (a) at a 5 mm distance from the external antenna plane, for the real-multiple-turn and annular geometries, and (b) at a 1 mm distance from the internal antenna plane for the real-multiple-turn and annular geometries.

3. Results

Regarding the problem presented in section 2.5, the **E**-field magnitude obtained with FEM was compared with the analytical solution. The error in the peak was found to be 7.50% at a 1.2 mm distance from the coil plane, 9.00% at 2.4 mm and 8.00% at 3.6 mm.

Regarding assessment of the error produced by the annular coil simplification, the normalized **E**-field magnitude at a 5 mm distance from the external antenna plane, is compared in figure 5a for the real-multiple-turn geometry and the annular geometry. In analogy, figure 5b compares the normalized **E**-field magnitudes at a 1 mm distance from the internal unit antenna, when exposed to the EMF created by the external-annular antenna. In both figures the error in the peaks was lower than 3%.

SAR distribution in an implanted subject is shown in figure 6. The excitation magnetomotive force in the external antenna, needed to induce the minimum operation current in the internal antenna, was 1.24 ampere-turn. Maximum SAR_{10} value was reached in the eyebrow, and equaled 0.024 W/kg. Furthermore, figure 7 compares average absorption rate in each ocular structure in the implanted and non-implanted subject. SAR values in the non-implanted subject were between 0.2-2% lower than the implanted subject, except in the orbital fat where it was about 1% bigger.

Regarding temperature rise, in order to compare experimental results and FEM results, the latter were scaled to produce the same magnetomotive force in the external

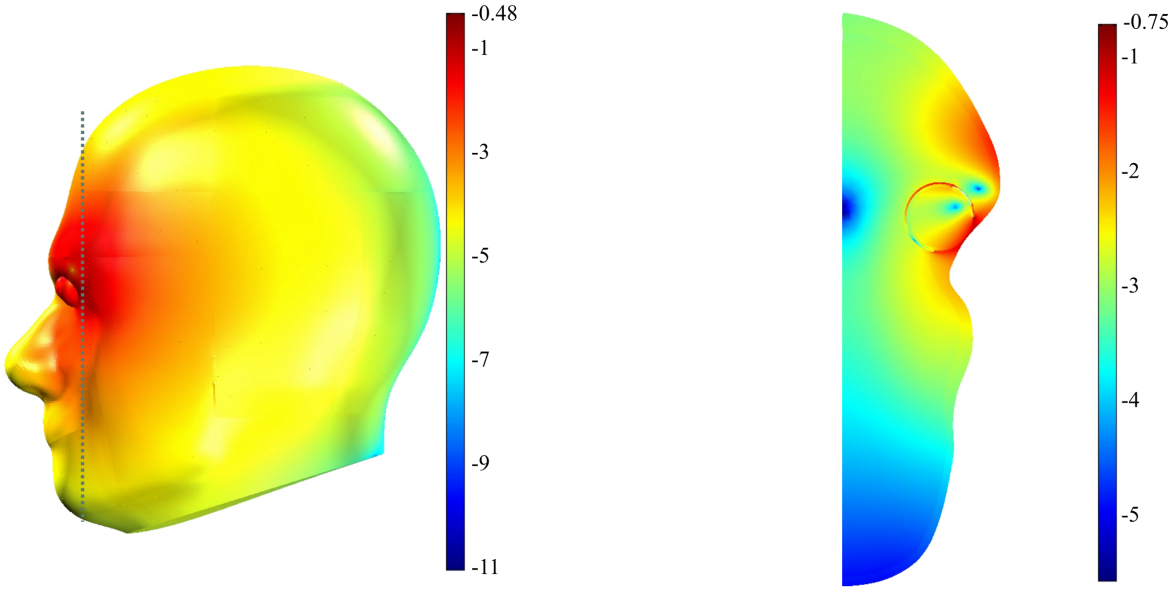

Figure 6: $\log_{10}(\mathrm{SAR/MMF^2})$ [W/kg/ampere-turn^2] distribution. (a) Lateral view and (b) slice view. The slice shown is indicated in figure 6a with a dashed-grey line.

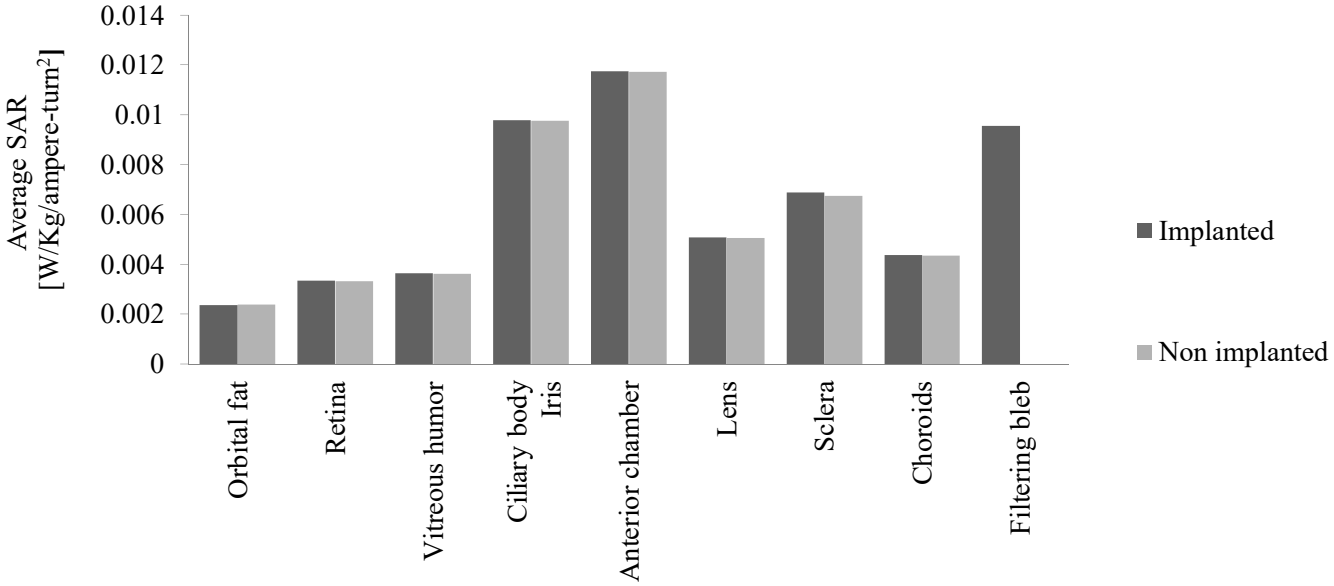

Figure 7: Average electromagnetic energy absorption rate in different ocular structures in both implanted and non-implanted subjects.

antenna. That is, SAR distribution was re-obtained using an external unit antenna excitation of 0.44 ampere-turn. Temperature distribution was calculated for that exposure. Maximum ΔT values were 0.007 °C and 0.006 °C, and occurred at the cornea and eyebrow respectively, as shown in figure 8.

Respecting basal temperature distribution, average corneal basal measured

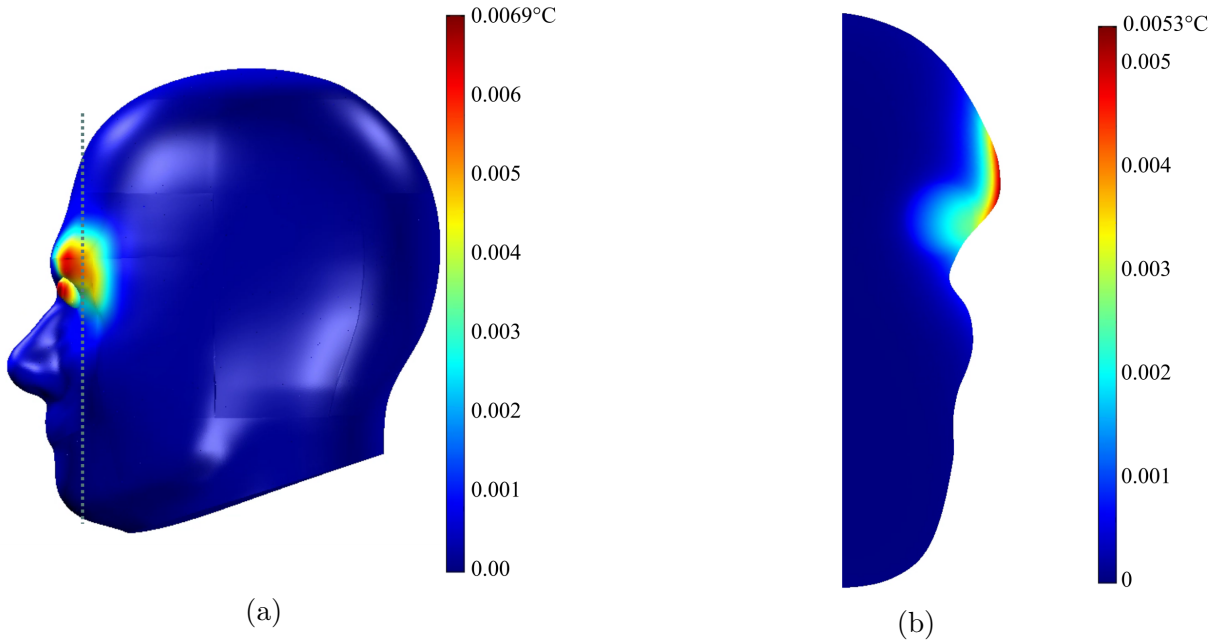

(a) (b)

Figure 8: ΔT distribution. (a) Lateral view and (b) slice view. The slice shown is indicated in figure 8a with a dashed-grey line.

temperature was T_{av} = 34.66 °C, and its standard deviation SD = 1.4 °C. Basal corneal temperature obtained with the described model was T_{FEM} = 32.05 °C, that is a -7.53% error. With regard to the in vivo experience, ΔT measurements in the four rabbits were averaged. No significative average ΔT could be appreciated, although standard deviation was high (0.67 °C). The study of the mesh showed that solution converges rapidly to the solution of mesh N°5, the most refined. After mesh N°2, the error remained below 2.5%.

4. Discussion

A 3D anatomical model was developed to assess thermal effects due to exposure to the EMF of the external unit of the microvalve.

Results presented were obtained using an excitation current in the external antenna, causing the minimum operation current in the internal unit antenna. When the minimum current is induced, the power dissipated by the implant is approximately 2 mW, but the power dissipated by the entire system is about 800 mW. If all this power was applied in a 10 g cube, which would be the worst situation, SAR_{10} would be 80 W/kg. This means that the microvalve system cannot be considered inherently safe, and a dosimetric study is needed. Furthermore, the external unit may not be used at the lower operation point, for example, to guarantee the functioning of the valve when the distance between antennae increases, due to human operation of the external unit. Regarding dosimetry, the upper limit for the external antenna current is given by SAR_{10}, which, as said, should remain below 2 W/kg. This SAR_{10} value is reached when

exciting the external antenna with a 11.3 ampere-turn magnetomotive force. In this case, the power dissipated is even bigger. This makes the presented dosimetric study even more necessary. The driving current for the external antenna should be chosen to be somewhere in the middle of the mentioned upper and lower limits.

SAR_{10} calculated values obtained with the lower excitation current, were significantly lower than the limits recommended by IEEE and ICNIRP standards not to be exceeded for general public exposure. But even with a current generating the maximum allowable SAR_{10}, according to ICNIRP (1998), temperature rises are not expected to cause a 41°C temperature in the lens, or a 36000 W/m^2 power density in the retina. This means that none of the established adverse effects is expected to occur neither in the eye nor in other tissue.

Additionally, as shown in figure 7, the eye structures absorbing electromagnetic energy at the highest rate were the aqueous humor in anterior chamber and in the filtering bleb, and the iris and ciliary body. This is due to their high electrical conductivity and closeness to the external unit. This result confirms that the inclusion of the filtering bleb was relevant. Anyway, after comparing results from the implanted and non-implanted subjects exposure in figure 7, it was found that, if the filtering bleb area is not considered, there is almost no difference between both scenarios, meaning that the presence of the internal unit modifies negligibly SAR distribution. Furthermore, as seen in figure 8, temperature rise is maximum in the closest points to the external unit, suggesting that ohmic heating in the internal unit is not important when compared to the heating produced by the external unit EMF. This means that the effect of the filtering bleb and implantable unit is local, and losses relevance at short distances.

Several studies were carried out to validate the obtained results. The comparison between FEM and analytical results in section 2.5 showed that FEM converges to a solution slightly bigger than the analytical, providing a safety margin to the dosimetric study. The mesh convergence study showed that results obtained, do not depend significantly on the mesh used. Regarding corneal basal temperature, FEM results were in acceptable agreement with experimental results of other authors. Finally, experimental temperature measurements in rabbits gave no appreciable ΔT. A possible explanation is that ΔT was smaller than NTC accuracy. This is compatible with FEM results where maximum ΔT is about ten times smaller than the used NTC accuracy. Nonetheless, a more probable explanation is related to noise. The air conditioner, the movement of people and the equipment present at the operating room, produced complex air streams that might have affected the NTCs in a different manner. Thus, these noise sources were not completely eliminated by the NTC differential configuration, and masked the real ΔT. This rationale is supported by the high dispersion in the data obtained experimentally. Besides, the number of rabbits available was not big enough to make a robust statistical analysis. Anyway, the experimental results were compatible with FEM results, and do not provide evidence about a dangerous ΔT.

Finally, the annular coil simplification in the internal and external antennae introduced a negligible error in the **E**-field distribution, as seen in figure 5. This

approximation allows to treat the complex multiple turn 3D geometry of a coil antenna, as a simple surface, obtaining practically the same behavior than the real geometry, but significantly lowering the mesh requirements. To complete the representation of the antennae, proper boundary conditions needed to be used. Hence, the internal antenna surface was treated as a sheet impedance, and in the external antenna surface a superficial current was prescribed.

5. Conclusions

A dosimetric study for a novel implantable device for the treatment of glaucoma and its external powering unit was undertaken. Geometry of the model used for such dosimetric study differs from other reported dosimetric studies mainly in the inclusion of a filtering bleb.

Results obtained show that, regarding thermal effects, the analyzed device is safe to be operated when exposed to its external unit EMF. Simplifications made produced either a negligible error, or a conservative model, overestimating SAR obtained values. Comparisons carried out for validation purposes gave reasonable concordance with numerical results. The exception were *in vivo* results, which were not clear enough. Anyway, they do add up arguments to the fact that no dangerous ΔT occurs due to exposure to the EMF produced by the external unit antenna.

Also, as a result of the dosimetric study, it was found high local absorption in the bleb area, meaning that including this structure was necessary for representing the phenomenon properly. New implants for the treatment of glaucoma are under development. Some of them might involve the creation of a filtering bleb, and it is reasonable assume that they will also involve exposure to EMF for powering and/or data transmission. This dosimetric study sets a precedent for such new devices.

Finally, exposure of a person wearing the microvalve to EMF sources other than the external unit, such as mobile phones, wireless networks, electric power lines, surveillance systems, domestic appliances among other, should also be accounted for in the future.

Acknowledgments

Authors would like to thank ANPCyT and CONICET for supporting this research, and the collaboration of the Biomecánica Computacional group at FI-UNER, Argentina.

References

Bae B, Kee H, Kim S, Lee Y, Sim T, Kim Y & Park K 2003 *Journal of Micromechanics and Microengineering* **13**(5), 613.

Bernardi P, Cavagnaro M, Pisa S & Piuzzi E 1998 *Microwave Theory and Techniques, IEEE Transactions on* **46**(12), 2074–2082.

Buccella C, De Santis V & Feliziani M 2007 *in* 'Electromagnetic Compatibility, 2007. EMC 2007. IEEE International Symposium on' IEEE pp. 1–6.

DeMarco S C, Lazzi G, Liu W, Weiland J D & Humayun M S 2003 *Antennas and Propagation, IEEE Transactions on* **51**(9), 2274–2285.

Diouf A, Reimann G & Bifano T 2008 *Journal of Micro/Nanolithography, MEMS, and MOEMS* **7**(3), 030501–030501.

Elder J 2003 *Bioelectromagnetics* **24**(S6), S148–S161.

Goel M, Picciani R G, Lee R K & Bhattacharya S K 2010 *The open ophthalmology journal* **4**(1).

Gosalia K, Weiland J, Humayun M & Lazzi G 2004 *Biomedical Engineering, IEEE Transactions On* **51**(8), 1469–1477.

Greenfield D S, Liebmann J M, Jee J & Ritch R 1998 *Archives of Ophthalmology* **116**(4), 443–447.

Guarnieri F A 2012 'Implantable ocular microapparatus to ameliorate glaucoma or an ocular overpressure causing disease'. US Patent 8206440.

Hirata A 2005 *Electromagnetic Compatibility, IEEE Transactions on* **47**(1), 68–76.

Hirata A, Matsuyama S i & Shiozawa T 2000 *Electromagnetic Compatibility, IEEE Transactions on* **42**(4), 386–393.

Hirtl R & Schmid G 2013 *Physics in medicine and biology* **58**(18), N267.

ICNIRP 1998 *Health Phys* **74**(4), 494–522.

IEEE 2003 Recommended Practice for Determining the Peak Spatial-Average Specific Absorption Rate (SAR) in the Human Head from Wireless Communications Devices: Measurement Techniques Standard The Institute of Electrical and Electronics Engineers, Inc. (IEEE).

IEEE 2005 Standard for Safety Levels with Respect to Human Exposure to Radio Frequency Electromagnetic Fields, 3 kHz to 300 GHz Standard The Institute of Electrical and Electronics Engineers, Inc. (IEEE).

IFAC 1997 An Internet resource for the calculation of the dielectric properties of body tissues in the frequency range 10 Hz-100 GHz Internet document Italian National Research Council - Institute for Applied Physics.

Jin J M 2002 *The finite element method in electromagnetics* John Wiley & Sons.

Kuo A 1999 *Polymer data handbook* Oxford University Press Oxford.

Lazzi G 2005 *Engineering in Medicine and Biology Magazine, IEEE* **24**(5), 75–81.

Lide D R 2004 *CRC handbook of chemistry and physics* Vol. 85 CRC press.

Lim K, Allan B, Lloyd A, Muir A, Khaw P, Lim K, Allan B, Lloyd A, Muir A & Khaw P 1998 *British journal of ophthalmology* **82**(9), 1083–1089.

Margalit E, Maia M, Weiland J D, Greenberg R J, Fujii G Y, Torres G, Piyathaisere D V, O'Hearn T M, Liu W, Lazzi G et al. 2002 *Survey of ophthalmology* **47**(4), 335–356.

Neagu C R 1998 A Medical Microactuator Based on an Electrochemical Principle PhD thesis Twente University.

Ng D C, Wang X, Felic G K, Bai S, Boyd C S, Halpern M & Skafidas E 2011 *in* 'EMC Europe 2011 York' IEEE pp. 79–83.

Ng E & Ooi E H 2007 *Computers in biology and medicine* **37**(6), 829–835.

Pan T, Baldi A & Ziaie B 2007 *Biomedical microdevices* **9**(3), 385–394.

Sassetti F, Guarnieri F, Garelli L & Storti M 2012 *Computer methods in biomechanics and biomedical engineering* **15**(12), 1273–1280.

Schwartz K S, Lee R K & Gedde S J 2006 *Current opinion in ophthalmology* **17**(2), 181–189.

Singh V, Qusba A, Roy A, Castro R, McClure K, Dai R, Greenberg R J, Weiland J D, Humayun M S, Lazzi G et al. 2009 *Antennas and Propagation, IEEE Transactions on* **57**(10), 3110–3118.

Stergiopulos N 2016 'Non-invasively adjustable drainage device'. US Patent App. 15/019,890.

Taflove A & Brodwin M E 1975 *Microwave Theory and Techniques, IEEE Transactions on* **23**(11), 888–896.

Torres R M & Guarnieri F A 2015 *Investigative Ophthalmology & Visual Science* **56**(7), 2697–2697.

Vander Vorst A, Rosen A & Kotsuka Y 2006 John Wiley & Sons chapter 3.6, pp. 120–122.

Weinreb R N, Aung T & Medeiros F A 2014 *Jama* **311**(18), 1901–1911.